 ICCES, vol.5, no.4, pp.199-204

Computational Flow Simulations around Circular Cylinders Using a Finite Element Method

Kazuhiko Kakuda[1], Masayuki Sakai[1] and Shinichiro Miura[2]

Summary

The applications of a finite element scheme to three-dimensional incompressible viscous fluid flows around circular cylinders are presented. The scheme is based on the Petrov-Galerkin weak formulation with exponential weighting functions. The incompressible Navier-Stokes equations are numerically integrated in time by using a fractional step strategy with second-order accurate Adams-Bashforth scheme for both advection and diffusion terms. Numerical solutions for flow around a circular cylinder are presented. The parallelization and the performance of the present scheme are also checked.

Introduction

In the flow field around a circular cylinder up to high Reynolds number, there are some interesting phenomena such as von Kármán vortex street, the decreasing of the drag coefficients on the cylinder, the transition from laminar flow to turbulence, and so forth. The studies of such flow phenomena have been qualitatively and quantitatively presented by many experimental fluid dynamicists [1-6] and computational fluid ones [7-9].

In our previous works, we have presented the Petrov-Galerkin finite element scheme using exponential weighting functions for solving effectively incompressible Navier-Stokes equations up to high Reynolds number regimes [10,11]. The finite element scheme was applied to three-dimensional flow around a circular cylinder within the wide range of Reynolds numbers from 10^3 to 10^6, and the agreement between the present results using coarse meshes and other existing data qualitatively appeared satisfactory [11].

The present work gives more quantitative agreement for the flow around a circular cylinder using the Petrov-Galerkin finite element scheme with finer meshes. The parallelization of the finite element scheme is also necessary to attempt the possibility to large-scale flow simulations. The parallel strategy utilized here is based on the well known domain-decomposition technique [12]. The parallel performance is also evaluated on PC cluster using MPI(Message-Passing Interface).

Petrov-Galerkin Finite Element Formulation

The motion of an incompressible viscous fluid flow is governed by the Navier-Stokes equations in dimensionless form. By applying the time splitting technique

[1]Department of Mathematical Information Engineering, College of Industrial Technology, Nihon University, Chiba 275-8575, Japan. E-mail: k7kakuda@cit.nihon-u.ac.jp

[2]Department of Mechanical Engineering, Tokyo Metropolitan College of Technology, Tokyo 140-0011, Japan

to the set of equations, we can split formally the problem into the nonlinear system of advection-diffusion equations and the linear Euler's system of equations.

It is well known that the conventional Galerkin finite element scheme using coarse meshes leads to spurious oscillatory solutions for flow simulations at high Reynolds number. Therefore, let us now consider the Petrov-Galerkin finite element formulation using exponential weighting functions [10,11] to the nonlinear advection-diffusion equations with a Reynolds number Re. By applying the divergence theorem to the weighted residual form in a subdomain Ω_e of the whole domain Ω, and after some manipulations, we have the following weak form :

$$\int_{\Omega_e} \left\{ \dot{u}_i(\tilde{u}_i, u_i^n) + u_j u_{i,j} \right\} M_\alpha d\Omega + \int_{\Omega_e} \frac{1}{Re} u_{i,j} N_{\alpha,j} d\Omega = \int_{\Gamma_e} \tau_i N_\alpha d\Gamma \qquad (1)$$

where $\tau_i \equiv u_{i,j} n_j / Re$, Γ_e is the boundary on the subdomain, and M_α denotes the weighting function given by

$$\left.\begin{aligned} M_\alpha(x) &= \sum_{\gamma,i} N_\alpha(x) e^{-a_i(N_\gamma x_i^\gamma - x_i^\alpha)} \\ a_i &= \frac{\alpha_i}{|L_i|} sgn(v_i) \end{aligned}\right\} \qquad (2)$$

where N_α is the shape function in three dimensions, v_i is the velocity vector averaged in Ω_e, L_i is the reference length for x_i-directions, α_i is the upwinding parameters which control an effect of the upwinding, and $sgn(v_i)$ denotes the signum function.

At this stage, by using the second-order accurate Adams-Bashforth strategy as a time integration scheme, we have the finite element system of equations [11].

Numerical Examples

In this section we present numerical results obtained from applications of the above-mentioned numerical method to incompressible viscous flow problems. In our numerical performances, we adopt the lowest interpolation functions in which the velocity and the scalar potential are piecewise trilinear, and the pressure is constant over each element. The initial velocities are assumed to be zero everywhere in the interior domain.

Flow around a circular cylinder

We shall consider the flow around a circular cylinder as a typical flow problem. The whole domain consists of $30D$ in x_1-direction (i.e., the streamwise), $20D$ in x_2-direction (i.e., the lateral), and $4D$ in x_3-direction (i.e., the spanwise), where D is the diameter of the cylinder. The inflow is uniformly given as the velocity, U_0, without a velocity fluctuation. At the outflow boundary, we set $\phi = 0$ as the condition of the modified velocity potential ϕ and $\tau_i^n = 0$. The slip boundary conditions are used

on the lateral, the upper and lower boundaries, and non-slip conditions on the surface of the cylinder. The Reynolds number,Re, based on the uniform velocity,U_0, at the inflow and the diameter,D, of the cylinder is up to 10^6 in *case* 1. The parameters that characterize the finite element approximation are summarized in Table 1. The *case* 1 presented in reference [11] is the coarse meshes with 160×50 in the cross-sectional plane around the cylinder and 20 divisions in the spanwise direction. For the fine meshes in *case* 2 the number of meshes in the cross-sectional plane is 400×50 around the cylinder whereas the number of divisions in the spanwise direction is the same number as the *case* 1. Tables 2 and 3 give the computed time-averaged quantities for Reynolds numbers of 10^4 and 10^5, respectively, and compare with several experimental data and other numerical ones. In Tables 2 and 3, L_r/D denotes the recirculation length behind the cylinder, $\overline{C}_d$ the time-averaged drag coefficient, C_{pb} the back-pressure coefficient and S_t the Strouhal number. The present results of *case* 2 are fairly in good agreement with some experimental data. Fig.1 shows the instantaneous streamlines and pressure fields around the cylinder in the horizontal center cross-section for different Reynolds numbers. In Fig.2, we give the time-averaged pressure distributions along the surface of the cylinder for Reynolds numbers of 10^4 and 10^5, and also compare with the experimental data. The present profiles (see Fig.2(a)) of both cases agree generally well with the experimental data obtained by West and Apelt [3]. On the other hand, both profiles at $Re = 10^5$ are different in the interval $60^\circ < \theta < 300^\circ$. Especially the agreement between the present results in *case* 2 and the experimental data appears satisfactory around $\theta = 180^\circ$ behind the cylinder. Fig.3 shows the time-averaged drag coefficient, $\overline{C}_d$, and the Strouhal number, S_t, through comparison with experimental data and other numerical solutions. In case 1, the minimum value of the present drag coefficients is 0.4572 at $Re = 5 \times 10^5$. The correlation between the present results and some other data appears satisfactory except the solutions of 2D flow simulations up to Reynolds number of 10^4. The present results for the Strouhal number are also qualitatively similar to the experimental data.

Flow around two circular cylinders

As the second example, we shall consider the flow around two circular cylinders in order to check the parallelization of the finite element scheme using PC cluster. Table 4 gives the single processor specification used in this work. The characteristic parameters of the finite element discretization are summarized in Table 5. Fig.4 shows the decomposed meshes divided into 16 subdomains by using METIS [13] for three-dimensional flow around two circular cylinders at a Reynolds number of 10^3. The instantaneous streamlines and pressure fields using 1 processor shown in Fig.5(a) can be qualitatively compared with the results using 4 processors with different subdomains (see Fig.5(b), (c)). The workability of the paralleliza-

Table 1: A summary of the parameters

Cases	*Re*	Nodes	Elements	l_{min}	$\triangle t$	α_i
case 1[11]	$10^4, 10^5$	179,970	168,000	0.00341	0.002	0.4, 1.0
case 2	$10^4, 10^5$	449,610	420,000	0.00341	0.001	0.4

Table 2: Comparison of time-averaged quantities at $Re = 10^4$

	L_r/D	$\overline{C}_d$	C_{pb}	S_t
Presents				
case 1	0.765	1.227	-1.363	0.1984
case 2	0.750	1.184	-1.232	0.1977
Tamura&Kuwahara(1989)				
$FDM(400\times100\times40)$		≈ 1.193		
Experiments				
West&Apelt(1982)		≈ 1.18	≈ -1.22	≈ 0.199
Roshko(1954)		1.15	≈ -1.08	≈ 0.2
Fey et al.(1998)				0.1996

Table 3: Comparison of time-averaged quantities at $Re = 10^5$

	L_r/D	$\overline{C}_d$	C_{pb}	S_t
Presents($Re = 10^5$)				
case 1	0.529	1.027	-0.9835	0.1907
case 2	0.482	1.199	-1.247	0.1831
Tamura&Kuwahara(1989)				
$FDM(400\times100\times40)$		≈ 1.228		
Breuer(2000)				
$LES(325\times325\times64)$	0.375	1.286	-1.480	0.203
Experiments				
Cantwell&Coles(1983)	≈ 0.44	1.237	-1.21	0.179
Wieselsberger(1921),				
Schewe(1983)		≈ 1.2		≈ 0.2
Fey et al.(1998)				0.1846

tion to the present scheme is performed because the results using 4 processors are close to ones using 1 processor. Fig.6 shows the relationship between the number of processors and the computing performance, and gives good parallel performance of the present scheme.

Conclusions

We have presented a finite element scheme for solving numerically three-dimensional incompressible flow around a circular cylinder up to high Reynolds number. The scheme was based on the Petrov-Galerkin finite element formulation using ex-

Table 4: PC specification

Single processor	
CPU	Core2 Duo(E6600) 2.4GHz
Memory	1.0GB
Cashe	4MB
OS	Linux kernel2.6.18 (Fedora Core 5)
Number of processors	4

Table 5: A summary of the parameters

Re	Nodes	Elements	$\triangle t$	α_i
10^3	76,342	68,536	0.01	0.4

ponential weighting functions. The set of equations was numerically integrated in time by using the second-order accurate Adams-Bashforth strategy for both advection and diffusion terms. The numerical results for flow around a circular cylinder using fine meshes demonstrated more quantitative agreement with experimental data and other numerical ones.

The parallel computation of flow around two circular cylinders for example, has been also performed on a PC cluster equipped with four $Intel\ Core2\ Duo\ 2.4GHz$ processors. For the parallel implementation, the presented results demonstrated the efficiency and scalability of the parallelization using the domain-decomposition strategy.

References

1. Wieselsberger, C. (1921): "Neuere Feststellungen über die Gesetze des Flüssigkeits-und Luftwiderstands", *Phys. Z.* **22**, pp.321-328.
2. Roshko, A. (1954): "On the Drag and Shedding Frequency of Two-Dimensional Bluff Bodies", *NACA TN 3169*.
3. West, G.S.; Apelt, C.J. (1982): "The Effects of Tunnel Blockage and Aspect Ratio on the Mean Flow past a Circular Cylinder with Reynolds numbers between 10^4 and 10^5", *J. Fluid Mech.* **114**, pp.361-377.
4. Schewe, G. (1983): "On the Force Fluctuations Acting on a Circular Cylinder in Crossflow Form Subcritical up to Transcritical Reynolds Numbers", *J. Fluid Mech.* **133**, pp.265-285.
5. Cantwell, B.; Coles, D. (1983): "A Experimental Study of Entrainment and Transport in the Turbulent near Wake of a Circular Cylinder", *J. Fluid Mech.* **136**, pp.321-374.
6. Fey, U, König, M.; Eckelmann, H. (1998): "A New Strouhal-Reynolds-Number Relationship for the Circular Cylinder in the Range $47 < Re <$

2×10^5", *Phys. Fluids* **10**(7), pp.1547-1549.

7. Tamura, T.; Kuwahara, K. (1989): "Direct Finite Difference Computation of Turbulent Flow around a Circular Cylinder", *Num. Meths. Fluid Dyns.*, (Eds., M. Yasuhara *et al.*), pp.645-650.
8. Kashiyama, K.; Tamai, T.; Inomata, W.; Yamaguchi, S. (1998): "A Parallel Finite Element Method for Incompressible Navier-Stokes Flows Based on Unstructured Grid", *4th Japan-US Symp. F.E.M. in Large-Scale Computational Fluid Dynamics*, pp.21-24.
9. Breuer, M. (2000): "A Challenging Test Case for Large Eddy Simulation: High Reynolds Number Circular Cylinder Flow", *Int. J. Heat and Fluid Flow* **21**, pp.648-654.
10. Kakuda, K.; Tosaka, N. (1992): "Finite Element Approach for High Reynolds Number Flows", *Theoretical and Applied Mechanics*, **41**, pp.223-232.
11. Kakuda, K.; Miura, S.; Tosaka, N. (2006): "Finite Element Simulation of 3D Flow around a Circular Cylinder", *Int. J. Comp. Fluid Dyns.* **20**(3-4), pp.193-209.
12. Farhat, C.; Lesoinne, M. (1993): "Automatic Partitioning of Unstructured Meshes for the Parallel Solution of Problems in Computational Mechanics", *Int. J. Numer. Methods Eng.* **36**, pp.745-764.
13. Karypis Lab.: http://glaros.dtc.umn.edu/gkhome/views/metis

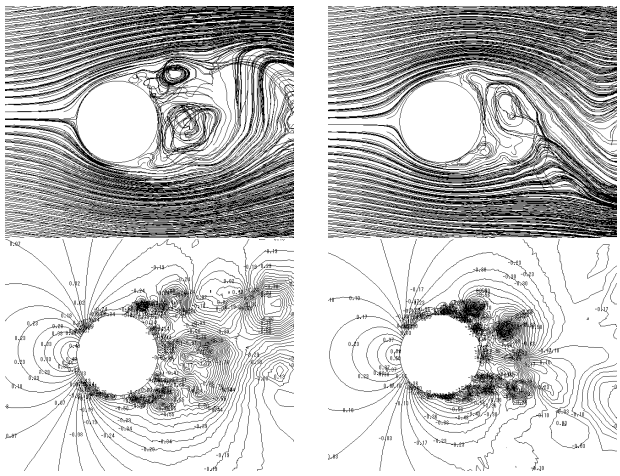

(a) $Re = 10^4$ (b) $Re = 10^5$

Figure 1: Instantaneous streamlines and pressure fields (*case* 2)

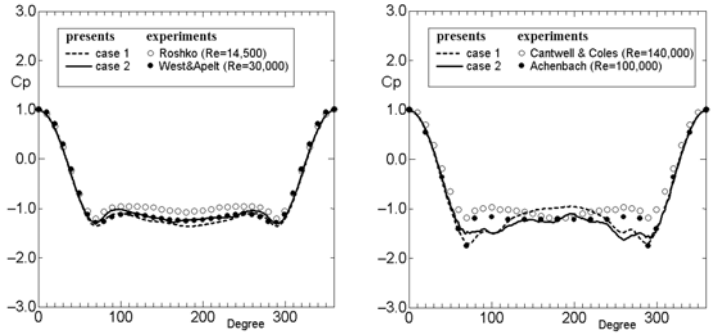

(a) $Re = 10^4$ (b) $Re = 10^5$

Figure 2: Time-averaged pressure distributions

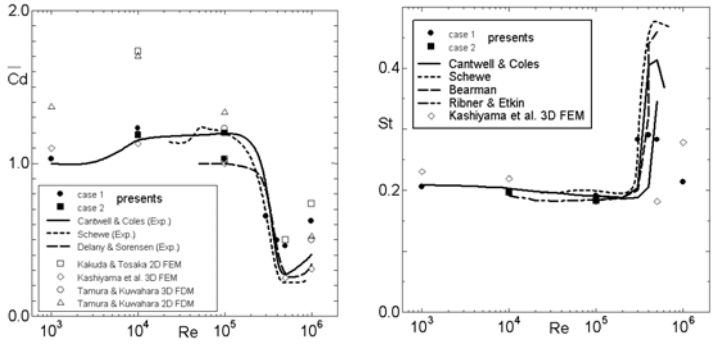

(a) Drag coefficients (b) Strouhal numbers

Figure 3: Time-averaged drag coefficients and Strouhal numbers

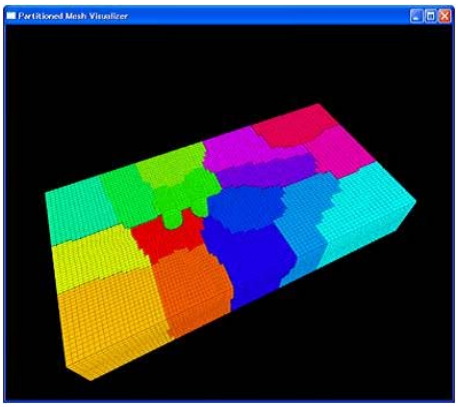

Figure 4: Domain-decomposition into 16 subdomains

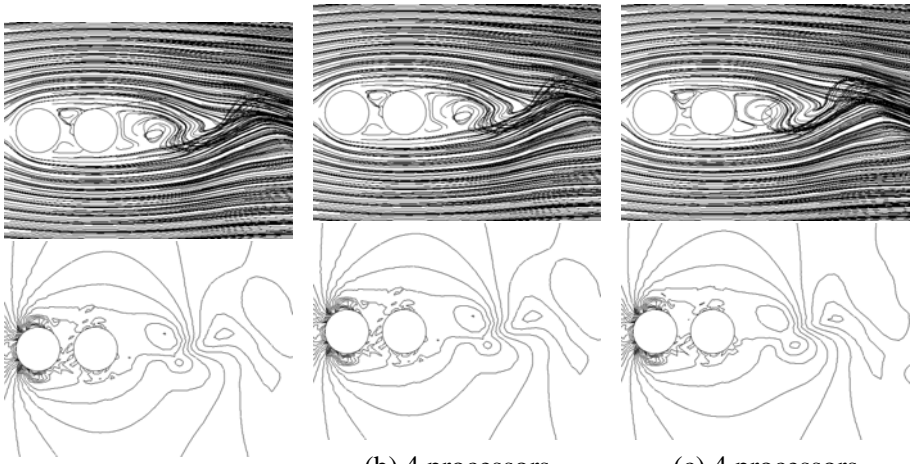

(a) 1 processor (b) 4 processors (4 subdomains) (c) 4 processors (16 subdomains)

Figure 5: Instantaneous streamlines and pressure fields at $Re = 10^3$

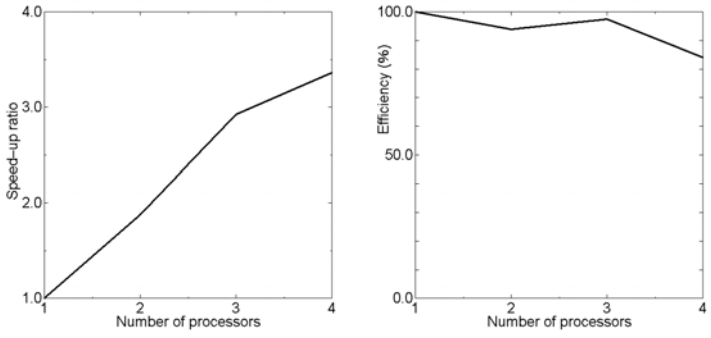

(a) Speed-up ratio (b) Efficiency

Figure 6: Parallel computing performances